Journal of Cleaner Production 393 (2023) 136350

Contents lists available at ScienceDirect

Journal of Cleaner Production

journal homepage: www.elsevier.com/locate/jclepro

Non-bituminous binders formulated with bio-based and recycled materials for energy-efficient roofing applications

R. Álvarez-Barajas, A.A. Cuadri *, C. Delgado-Sánchez, F.J. Navarro, P. Partal

Pro²TecS-Chemical Process and Product Technology Research Centre, Department of Chemical Engineering, ETSI. Campus de "El Carmen", Universidad de Huelva, 21071, Huelva, Spain

ARTICLE INFO

Handling Editor: Cecilia Maria Villas Bôas de Almeida

Keywords:
Non-bituminous binders
Roofing
Building energy-efficient
Rheology
Product engineering

ABSTRACT

Non-bituminous binders have been designed as potential roofing materials with sustainable characteristics. To that end, three bio-based rosin esters (R), a waste cooking oil (O) and a recycled polyethylene from greenhouse agriculture ($LDPE_r$) have been used in their formulations. A comprehensive rheological, microstructural, calorimetric, and technological characterization have been performed on binary (polymer/oil or rosin/oil) and ternary (polymer/rosin/oil) blends, allowing the compatibility among binder compounds to be studied. Additionally, thermal conductivity and solar radiation tests have been conducted on a selected non-bituminous binder and compared with a reference polymer modified bitumen. The formulation composed of 61.0% phenolic-modified rosin, 30.5% oil and 8.5% $LDPE_r$ has shown suitable mechanical properties for roofing materials, and has exhibited enhanced energy efficiency derived from its light yellowish to brownish color. Under the experimental radiant flux conditions, surface temperature of the non-bituminous binder was 8 °C lower than that of the black bitumen. Moreover, conduction heat transfer through this roofing material was about 14% lower than that conducted through a bitumen-based membrane with the same thickness. Accordingly, developed binders are expected to behave as reflective building materials aiming to reduce the heat island effects and save energy.

1. Introduction

Polymer-based building materials can be classified in accordance with their applications as substrates, coatings and binders, where bitumen is mainly used as a binding material (Shen et al., 2020). Among them, non-bituminous materials are commonly made of synthetic resins, different fillers, plasticizers, curing agents, colorants or stabilizers (Wypych, 2020), where functional additives are added to extend material applications and enhance their performance and processability (Ebnesajjad and Morgan, 2012; Tolinski, 2009). Examples of such materials are polyester polymer concrete (PPC) (Ferdous et al., 2016), fiber reinforced polymers (FRPs), glass fiber reinforced polymers (GFRPs) and even the more traditional pre-packaged polymer modified slurries (PPPMS) (Iqbal et al., 2019) or pre-applied bonded waterproofing membranes of polyvinylchloride (PVC), thermoplastic and flexible polyolefins and ethylene-propylene-diene rubber (EPDM), which are bonded to concrete (Muruzina and Murzagalina, 2020).

Among waterproof coating materials, bitumen felts have been the most common and widespread roofing and waterproofing products over the years. For these materials, bitumen modification by polymers is a must in order to meet increasing requirements for performance and durability (Burkhanovich, 2022; Shen et al., 2020; Okhotnikova et al., 2022). Thus, virgin and recycled polymers have stablished themselves as bitumen additives, preventing its main in-service distresses (Fuentes-Audén et al., 2008; Kazemi and Fini, 2022; Navarro et al., 2010; Okhotnikova et al., 2022).

Although numerous bitumen substitutes have been suggested due to its intrinsic disadvantages, very few formulations exclude bitumen entirely (Iqbal et al., 2019), being styrene-butadiene-styrene (SBS) modified bitumen membranes and atactic polypropylene (APP) modified the most common waterproofing membranes in the European market (Garrido et al., 2018; Rupal et al., 2020; Shen et al., 2020). Furthermore, polymer modified bitumen membranes (PBMs) have been formulated with virgin or waste styrene-butadiene-styrene (SBS) and polyphosphoric acid (PPA), ethylene-vynil-acetate (EVA), ethylene-butyl-acrylate (EBA) (Senise et al., 2017), both high and low density polyethylene (HDPE & LDPE) (Okhotnikova et al., 2022), polyethylene wax (PW) (Munera and Ossa, 2014), polyurethane (PU)

* Corresponding author.
E-mail address: antonio.cuadri@diq.uhu.es (A.A. Cuadri).

https://doi.org/10.1016/j.jclepro.2023.136350
Received 16 October 2022; Received in revised form 17 January 2023; Accepted 3 February 2023
Available online 6 February 2023

(Rupal et al., 2020) and crumb or liquid rubber CR (Fuentes-Audén et al., 2007; Navarro et al., 2010), most of them coated on reinforcing carrier layers to give consistency and to ease the application.

However, green construction pursues the development and instauration of environmentally friendly construction practices that reduce pollutants and materials usage, and promote the re-use and recycle of materials, energy savings, environmental preservation and sustainability (Bianchini and Hewage, 2012; Zakaria et al., 2018). Likewise, roof performance over time and the disposability at the end of its lifecycle is also a crucial issue in its development to promote new circular economy strategies (Muruzina and Murzagalina, 2020). In this scenario, non-bituminous binders have been proposed as an alternative to petroleum-originated bitumen. Their formulation (e.g. composed of oils from crude distillation, pine rosin and waste polyolefins or SBS) makes them greener and, furthermore, easily pigmentable due to the lack of black asphaltenes present in bitumen (Fuentes-Audén et al., 2007; Navarro et al., 2005). This feature may represent a valuable advantage for the development of strategies seeking reduction of solar heating in urban environments, in accordance with the "cool roof" concept (Badin et al., 2021; Boixo et al., 2012). Sun radiation that hits the building surface may be reflected, absorbed, and finally transferred into it, affecting its habitability (Pan et al., 2022; Shittu et al., 2020). Roofing materials based on such non-bituminous binders may become a way to extend roof life and create a reflective surface that will comply with industry reflectivity requirements, reduce the heat island effect, and save energy.

Pursuing above green and saving objectives, this work addresses the design of novel non-bituminous binders as potential roofing materials with advanced sustainable and energy efficiency characteristics. For this purpose, bio-based rosin esters, a waste cooking oil and a polyethylene recycled from greenhouse agriculture have been used in their formulations.

It is well known that plastic wastes produce a major impact particularly on environment, especially those from agri-food industry (Cascone et al., 2020; Joni et al., 2020). On the other hand, waste vegetable oils produced after cooking and frying activities either in food industries or at consumer homes have become an important environmental pollutant (Brännström et al., 2018; Joni et al., 2020). Finally, the third component of non-bituminous binders was selected among rosin esters derived from pine resin that has been historically used in waterproofing, particularly in wooden ships (Silvestre and Gandini, 2008). Colophony rosin is composed of semi-volatile monoterpene hydrocarbons and small amounts of other neutral compounds and mainly, diterpeninc monocarboxylic acids (resin acids) that derive from three basic tricyclic carbon skeletons abietane, pimarane and isopimarane. Its derived rosin esters may improve thermo-physical, mechanical and functional properties of the final products, being commonly used in the manufacture of curing agents, elastomers, surfactants, coatings, adhesives and hardeners (Aldas et al., 2020; Kugler et al., 2019; Silvestre and Gandini, 2008).

With the specific objective of designing novel non-bituminous binders with improved sustainable and energy-efficient characteristics, this work addresses a comprehensive rheological, microstructural, calorimetric, and technological characterization performed on binary (polymer/oil or rosin/oil) and ternary (polymer/oil/rosin) blends. This study has provided an in-depth understanding of the role of the three compounds in the final material performance, allowing the binder composition to be optimized. Additionally, thermal conductivity and solar radiation tests have been conducted on a selected non-bituminous binder and compared with a reference polymer-modified bitumen. The resulting binders may provide a greener and eco-friendlier alternative to traditional petroleum-derivatives.

2. Materials and methods

2.1. Raw materials and formulations

Binders were formulated using three modified bio-based rosin esters obtained from pine trees and supplied by Luresa, S.A (Spain); a recycled low-density polyethylene ($LDPE_r$) supplied by Reciclados Nijar (Spain); and a recycled vegetable cooking oil supplied by BIOLIA, S.A (Spain). Most significant rosin ester characteristics are summarized in Table 1.

Model binary polymer (P) and oil (O) blends were prepared, containing different polymer/oil ratios (from 0.05 to 0.3), to evaluate compatibility between both compounds and to evaluate the waste oil as potential non-polar swelling agent of polyethylene molecules. Likewise, waste oil affinity with rosin esters (R) was studied at a constant rosin/oil ratio of 3/1. Subsequently, ternary blends were prepared with R/O ratios from 0.4 to 3.0 and keeping P/O ratios between 0.25 and 0.28. However, as will be discussed later, only ternary blends formulated with RPH or RSA are stable, since RML/O/P blends undergo a fast polymer phase separation just after processing.

Finally, based on the results obtained from ternary blends, Table 3 gathers the model binder formulations proposed as binders with potential use in roofing applications, according to standard ASTM D312 and their rheological response. These ternary blends display rosin/oil ratios between 2/1 and 3/1 and two polymer/oil ratios (0.19 and 0.28).

2.2. Processing and testing methods

Samples were prepared in a Silverson L5 Laboratory mixer using a squared hole high shear screen at 180 °C, 3800 rpm agitation speed, and using different mixing times depending on the preparation. Binary polymer-oil blends were processed for 180 min whereas rosin-oil blends were stirred for 30 min. For ternary blends, oil and rosin were initially mixed for 30 min and then polymer was added, being the total processing time limited to 180 min.

Rheological characterization consisted of oscillatory shear linear viscoelastic tests and steady viscous flow measurements. Temperature sweep tests in oscillatory shear were conducted between 30 and 140 °C in a SmartPave 102e rheometer (Anton Paar, Austria) with a plate-plate geometry (25 mm diameter and 1 mm gap) at 10 rad/s and 1 °C/min temperature ramp. Oscillatory frequency sweep tests, from 0.03 to 100 rad/s, were performed in a RheoStress RS600 rheometer (Thermo Haake, Germany) at 60 °C with a plate-plate geometry. Viscous flow tests, between 0.1 and 100 s^{-1}, were carried out in an Ares rheometer (Rheometrics Scientific, USA) using coaxial cylinder geometries at temperatures of 135, 165 and 180 °C.

Differential Scanning Calorimetry (DSC) analysis was carried out in a DSC TA Q100 (TA Instruments, USA) from −80 °C to 180 °C. Samples of 5–10 mg, placed into aluminum hermetic pans. After first heating up to 180 °C to avoid the effect of material past thermal history, DSC scans were obtained between −80 °C and 180 °C. The heating/cooling rate was set at 10 °C/min and 50 ml/min N_2 purge gas flow was used.

The sample morphology was observed in an Olympus BX51 optical microscope (Japan). Light transmission and polarized light micrographs

Table 1
Softening point and acid number of colophony rosin ester used (data provided by the producer).

Rosin	Type	Softening point [(1)] (°C)	Acid number [(2)] (mg KOH/g)
RSA	Pentaester of stabilized rosin acids	108	12
RML	Maleic-modified pentaerythritol ester of gum rosin	135	25
RPH	Phenolic-modified glycerolester of gum rosin	108	20

According to [(1)] ASTM E28 and [(2)] ASTM D465.

Table 2
Composition for ternary RPH/O/P and RSA/O/P blends.

Sample Rosin/ Oil/Polymer	Rosin (R) (%)	Oil (O) (%)	LDPE (P) (%)	R/ O	R/P	P/O
0.25P/O	0.00	80.00	20.00	0.0	0.00	0.25
0.4RPH/O-15.4% P	23.08	61.54	15.38	0.4	1.50	0.25
0.6RPH/O-13.8% P	32.30	53.91	13.79	0.6	2.34	0.26
1.1RPH/O-11.4% P	45.59	43.05	11.36	1.1	4.01	0.26
1.3RPH/O-10.7% P	49.67	39.66	10.68	1.3	4.65	0.27
1.8RPH/O-9.0%P	58.29	32.75	8.96	1.8	6.50	0.27
2.1RPH/O-8.1%P	62.43	29.45	8.12	2.1	7.69	0.28
2.7RPH/O-6.9%P	68.10	24.99	6.92	2.7	9.84	0.28
1.0RSA/O-11.5% P	44.18	44.29	11.53	1.0	3.83	0.26
1.3RSA/O-10.4% P	50.34	39.30	10.36	1.3	4.86	0.26
1.7RSA/O-9.1%P	57.18	33.72	9.10	1.7	6.28	0.27
2.1RSA/O-8.0%P	62.73	29.24	8.02	2.1	7.82	0.27
3.0RSA/O-6.6%P	70.10	23.29	6.60	3.0	10.62	0.28

Table 3
Model binder compositions and their penetrations (Pen.) values and softening points ($T_{R\&B}$).

Binder Sample	Rosin (R) (%)	Oil (O) (%)	LDPE (P) (%)	R/ O	P/O	Pen. [c] (dmm)	$T_{R\&B}$ [d] (°C)
B-2RML/ O-6.0% P	62.65	31.32	6.03	2	0.19	26 ± 2 [a]	59.1 ± 0.3 [a]
B-2RML/ O-8.7% P	60.88	30.44	8.68	2	0.28	[a]	120.0 ± 0.5 [a]
B-2.7RPH/ O-6.9% P	68.10	24.99	6.92	2.7	0.28	25 ± 2	49.2 ± 0.3
B-2RPH/ O-6.0% P	62.65	31.32	6.03	2	0.19	54 ± 4	108.5 ± 1.1
B-2RPH/ O-8.5% P	60.98	30.49	8.54	2	0.28	28 ± 2	109.1 ± 1.3
B-3.0RSA/ O-6.6% P	70.10	23.29	6.60	3	0.28	52 ± 3	53.7 ± 0.4
B-2RSA/ O-6.0% P	62.65	31.32	6.03	2	0.19	[b]	72.8 ± 0.7
B-2RSA/ O-8.7% P	60.88	30.44	8.68	2	0.28	[b]	101.7 ± 0.6

[a] Undergone quick polymer phase separation.
[b] Not measured. Measured according to.
[c] ASTM D5 and.
[d] ASTM D36.

were taken at room temperature. Samples were prepared in standard microscope slides (76 × 26 mm) at temperatures below the polymer melting point.

Oil retention capability of the polymeric matrix was studied at 4 different storage temperatures. About 2 g samples of the binary polymer-oil blends were poured into metallic pans and stored for 24 h at temperatures between −30 °C and 60 °C. After storage, polymer-oil phase was taken apart from the remaining oil, superficially dried and weighted. Oil retention was calculated as a percentage of the weight of the initial sample and the weight of the oil-retained in the polymer-rich fraction. Penetration and softening point technological test were performed on polymer-oil blends and final binder formulations according to ASTM D5 and D36 standards, respectively.

2.3. Thermal conductivity and heat radiation tests

The thermal conductivity at different temperatures was measured using the non-destructive Transient Hot-Bridge (THB) technique by a THB 100 device from Linseis GmbH (Germany). A sensor type A with a metal frame (A-13890) was used for the measurements. The sensor was placed between two equal flat faces of two samples (minimum sample size, 20 × 40 × 5 mm) of the same formulation and thermostatized in a lab Heratherm oven (Thermo Scientific, Germany). Ten replicas were recorded for each sample and temperature.

As for the simulated solar irradiation tests, samples were subjected to a constant incident radiation power by using a Xenon lamp HXF300-T3 (Beijing China Education Au-light Technology Co., Ltd, China), with an attached filter AM 1.5G (300–1100 nm). Testing specimens of 70 mm diameter and 5 mm thickness were obtained by pouring samples into a silicone mold with two temperature sensors located at the top and the bottom. The lamp power was adjusted to achieve mean incident irradiations of 924 ± 282 and 1266 ± 386 W/m^2, which vary with radius. A pyranometer SMP3 (Kipp & Zonnen, Netherlands) was used to measure the incident radiation. Temperature of the upper and lower surface of the sample was measured along time using two Pt-100 temperature sensors (0.8 mm diameter, and an accuracy of ±0.15 °C), being 4.54 mm the distance between them. Sample side wall was isolated, whereas its bottom side was in contact with a ceramic surface acting as heat sink. As a result, steady state conditions were reached, and one-dimensional heat conduction through material can be assumed. A commercial 45/80-75 SBS modified binder supplied by Repsol, S.A was used as reference material.

3. Results and discussion

3.1. Oil-polymer blends

As a first step in the design of the non-bituminous binders, waste vegetable oil was evaluated as potential non-polar swelling agent of polyethylene molecules, to form a polymer-rich (gel-like) material. Such a polymeric phase will be responsible for relevant in-service properties of the new binders requested in roofing applications (e.g. stiffness, softening point, low temperature flexibility, etc.) (Fuentes-Audén et al., 2008). To that end, compatibility between both compounds was evaluated by means of a rheological, technological, and calorimetric characterization of the processed polymer-oil blends for P/O ratios between 0.05 and 0.30.

Polymer is expected to be swollen by oil leading to oil retention (O_{ret}) that depends on both polymer concentration and storage temperature, as shown in Fig. 1A for P/O > 0.1. This was the lowest ratio able to form an extended three-dimensional polymeric network. As a whole, oil retention increases with polymer concentration, showing constant values of O_{ret} at −30 and 5 °C for P/O > 0.1. However, as temperature increases the differences between samples become greater, being maximum at the highest storage temperature evaluated, 60 °C (Fig. 1A). It has been reported that the interaction between oil and polyethylene increases with temperature, due to a higher molecular mobility. The presence of the solvent would induce the agglomeration of molecules of polymer, and a higher trend for oil separation (Rodríguez-Gómez et al., 2015).

Polymer swelling by oil is confirmed by differential scanning calorimetry (DSC) curves shown in Fig. 2. Pure $LDPE_r$ and recycled oil show endothermic events with characteristic temperatures (T_m), respectively located at −17.6 and 108.5 °C (Fig. 2A). These events are related to the melting process of their respective crystalline fractions (Li et al., 2019; Ribeiro et al., 2015). After blending, swollen $LPDE_r$ melting temperature drops to c. a. 101 °C, whereas waste oil endothermic peak is now located at c. a. −30 °C for all concentrations (Fig. 2B). The latter would correspond the melting of the reaming (non-absorbed) waste oil, as will be seen later. Therefore, compared with pure compounds, DSC

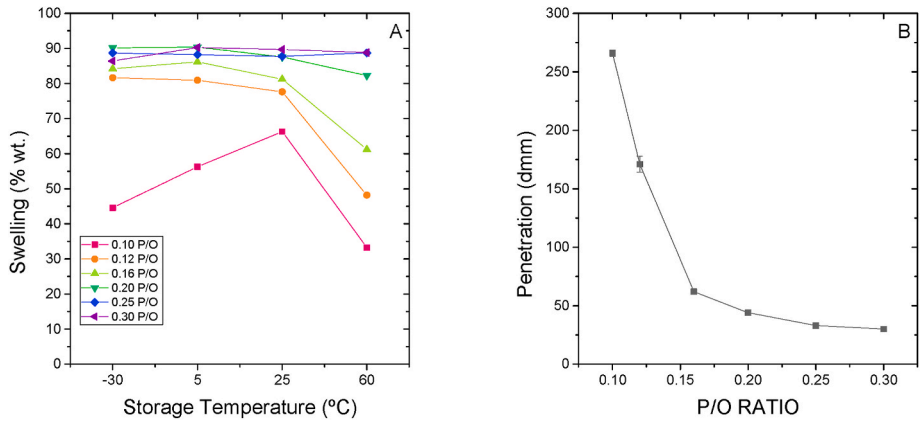

Fig. 1. A) Oil retained (O_{ret}) by polymer matrix as a function of storage temperature; and B) penetration for P/O blends (standard deviations are included).

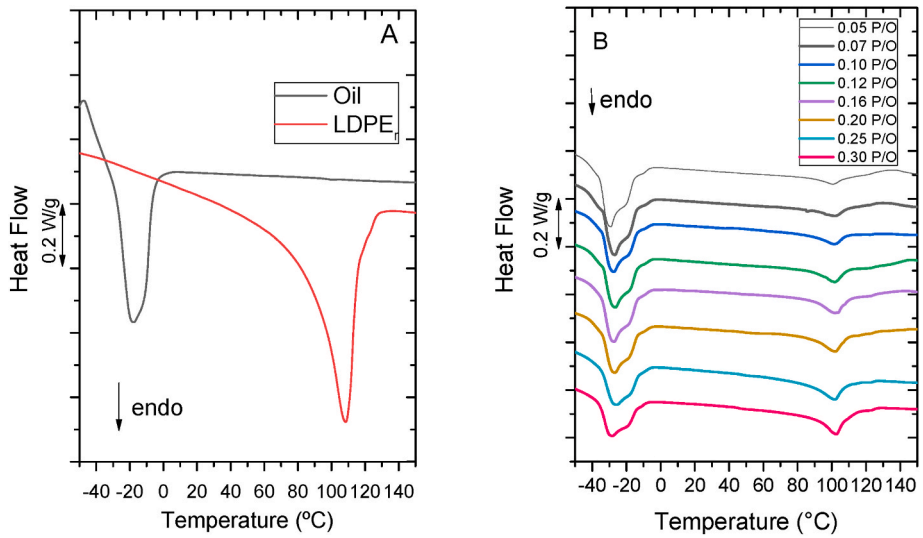

Fig. 2. DSC scans of: A) recycled LDPE and waste oil; and B) binary P/O blends.

endothermic events shifted to lower melting temperatures for both oil and $LDPE_r$ (about 12 °C and 8 °C, respectively), confirming polymer is being swollen by some fractions of waste oil. This fact also induces a change in the original polymer and oil crystallinities (Cuadri et al., 2016). In this regard, polymer crystalline fraction (X_c) was calculated as follows (Yuliestyan et al., 2018):

$$X_c(\%) = \frac{\Delta H_m}{293 \cdot C_{LDPE}} \cdot 100 \quad (1)$$

where ΔH_m (J/g) is the melting enthalpy taken from the second DSC heating ramp, 293 J/g is the melting enthalpy of a 100% crystalline polymer (Meisenheimer and Zens, 2008), and C_{LDPE} (−) is the polymer fraction in the sample. In addition, total crystalline fraction of LDPE, W_C (%), was calculated as $W_C = X_C \cdot C_{LDPE}$. According to Equation (1), swelling induced by oil leads to a significant reduction in X_C from 34%, for pure $LDPE_r$ to around 20%, measured for the swollen polymer, no matter concentration studied (Table 4).

On the other hand, unlike melting area of the swollen polymer that increases with P/O ratio, the melting area (or enthalpy) of the oil phase decreases as P/O is higher Fig. 2B. This fact points out a partial compatibility between the polymer and the oil, with the amount of free (non-absorbed) oil decreasing as the polymer concentration increases. As results, polymer would absorb only certain compounds of the aged oily fraction (likely, phospholipids, fatty acids, esters, etc.), which reduce crystallization degree of the swollen polymer respect to the reference $LDPE_r$ (see Xc values in Table 4).

However, stiffness of the polymeric matrix enhances as P/O ratio increases, as may be deduced from penetration tests performed on the polymer-rich phase (Fig. 1B). Thus, penetration results decrease with polymer concentration (i.e., polymeric phase becomes stiffer). Interestingly, penetration values obtained for P/O > 0.15 match those of bituminous binders typically used in commercial roofing membranes according to the ASTM D312. Conversely, materials become too soft at P/O ratios below 0.07 (i.e. penetration was higher 300 dmm), and are not presented in Fig. 1B. In agreement with O_{ret} results, penetration values decrease considerably up to P/O = 0.16, and level off for P/O = 0.25 and 0.30. This fact would suggest a maximum of polymer swelling has been reached at 0.25 P/O.

Stiffness of the polymer-rich phase was also studied as a function of temperature by dynamic shear temperature sweeps (Fig. 3A). Complex shear modulus (G*) decreases with increasing testing temperature from 30 to 140 °C. However, above 100 °C, G* sharply drops about three orders of magnitude in all cases. The temperature onset for this transition is related to melting (or collapse) of polymeric matrix, as may be deduced from the endothermic event shown in DSC curves (Fig. 2B), at a similar temperature.

Likewise, such a characteristic transition temperature is preceded by a maximum in the loss tangent curve (Tan δ = G”/G′) that is located at around 70 °C, close to onset of the DSC melting event, suggesting a change on polymer mobility that is able to store a higher amount of the

Table 4
Melting temperature (T_m), melting enthalpy (ΔH_m), degree of crystallinity (X_c) and total crystalline fraction (W_c) for P/O blends and final binders.

Polymer-oil BLENDS (P/O)	C_{LDPE} (−)	ΔH_m (J/g)	X_c (%)	$W_c = X_c{*}C_{LDPE}$ (%)	T_m (°C)
1	1.00	99.71 ± 1.41	34.0 ± 2.41	34.03 ± 2.41	108.5 ± 0.9
0.05	0.05	2.73 ± 0.41	19.5 ± 1.82	0.93 ± 0.25	100.8 ± 0.5
0.07	0.07	3.58 ± 0.31	18.7 ± 0.91	1.22 ± 0.46	100.6 ± 0.5
0.1	0.09	4.53 ± 0.62	17.0 ± 1.41	1.55 ± 0.31	100.8 ± 0.6
0.12	0.11	5.35 ± 0.38	17.0 ± 0.66	1.83 ± 0.39	100.4 ± 0.6
0.16	0.14	7.77 ± 0.54	19.2 ± 0.74	2.65 ± 0.41	100.2 ± 0.4
0.2	0.17	9.59 ± 0.81	19.6 ± 0.99	3.27 ± 0.54	101.3 ± 0.5
0.25	0.20	11.57 ± 0.67	19.7 ± 1.12	3.95 ± 0.84	100.8 ± 0.6
0.3	0.23	14.75 ± 1.06	21.8 ± 1.14	5.03 ± 0.58	100.9 ± 0.5
BINDERS					
B-2RML/O-6.0% P	0.06	5.65 ± 0.99	32.1 ± 1.84	1.93 ± 0.44	102.1 ± 0.6
B-2RML/O-8.7% P	0.09	8.34 ± 0.64	31.6 ± 1.38	2.85 ± 0.67	101.7 ± 0.4
B-2RPH/O-6.0% P	0.06	2.40 ± 0.74	13.6 ± 0.87	0.82 ± 0.28	100.7 ± 0.5
B-2RPH/O-8.5% P	0.09	3.15 ± 0.55	12.6 ± 0.74	1.08 ± 0.51	100.7 ± 0.6
B-2.7RPH/O-6.9%P	0.07	6.19 ± 0.64	30.5 ± 1.28	2.11 ± 0.64	101.7 ± 0.5
B-2RSA/O-6.0% P	0.06	2.14 ± 0.75	12.2 ± 0.88	0.73 ± 0.33	101.8 ± 0.5
B-2RSA/O-8.7% P	0.09	4.53 ± 0.63	17.8 ± 0.51	1.55 ± 0.51	101.7 ± 0.6
B-3RSA/O-6.6% P	0.07	4.28 ± 0.84	22.1 ± 0.99	1.46 ± 0.39	102.6 ± 0.5

stress applied at 10 rad/s (i.e. an enhancement of the elastic (G') versus the viscous (G") material response) (Yuliestyan et al., 2016, 2018). It is worth noting that oil retention tests showed an increase in oil release at 60 °C (Fig. 1A), which was higher as polymer ratio was lower. This release would induce an effective or local polymer concentration above this temperature that increases interaction among molecules and, therefore, material elasticity. Accordingly, the initially less concentrated system P/O = 0.1, but with the highest oil release at 60 °C, exhibited the highest elastic character or the lowest Tan δ values at around 105 °C (Fig. 3A). That behavior is observed till microstructure collapses (melts down), depending on the sample, in the range of 100–105 °C. Furthermore, Fig. 3A points out a prevailing elastic behavior in all samples below the melting point, and once the melting process is completed loss tangent presents value above unity (i.e. material exhibits a predominant viscous character).

Finally, the above-commented partial compatibility between polymer and oil affects blend viscous behavior at temperatures above the system melting point (Fig. 3B). Viscosity tests evidenced Newtonian flow behaviors for all P/O ratios at 165 and 180 °C, with viscosity values slightly dependent on temperature. Fig. 3B shows that polymer concentration is the main variable affecting blend viscosity that rises with P/O ratio.

3.2. Oil-resin blends

Viscosity tests on pure rosins were conducted at temperatures above their respective melting points shown in Table 1, exhibiting most samples an almost Newtonian response, as previously reported by Xu et al. (2019). For a selected shear rate of 100 s^{-1}, Fig. 4A, viscosity shows an Arrhenius-like dependence on temperature for all rosins. RML has the highest viscosity values at all temperatures tested, whereas RSA is slightly more viscous than RPH. Likewise, activation energies calculated from Arrhenius equation, and shown in Table 5, were similar to others measured in steady state viscous flow tests for bituminous and synthetic binders (Partal et al., 1999).

Oil-rosin blending at R/O = 3 leads to a drop in viscosity and activation energy values, and to a Newtonian response no matter the resin considered (Fig. 4A). Again, RML/O blend showed the highest viscosity, and differences between RSA and RPH disappear when mixed with oil. The use of pentaerythritol in resin esters such as RML and RSA had been previously reported as an adequate viscosity modifier that could also improve thermal stability and antioxidant characteristics of rosin blends (Xu et al., 2019).

These results suggest a high compatibility between waste cooking oil and rosin esters, which is confirmed by DSC tests (Fig. 4B and Table 5). Thus, DSC analysis shows glass transition temperatures (T_g) in pure resins between 60 and 70 °C that shifted to lower temperatures in R/O mixes (located around 10 and -15 °C). Results agree with those obtained by Fuentes-Audén et al. (2005) for blends of colophony rosin and a naphthenic oil from crude oil distillation, who reported a decrease in T_g with decreasing R/O ratio that was fitted to a Gordon-Taylor equation (Gordon and Taylor, 1952). Moreover, oil-resin blends do not show the low temperature melting event, previously related to the presence of free oil in the oil-polymer blend (Fig. 4B).

3.3. Oil-resin-polymer blends

Once binary P/O and R/O blends have been studied, ternary systems were evaluated aiming to assess the compatibility among the three compounds that eventually will form non-bituminous binders. To that end, increasing amounts of rosin were added to a selected polymer-oil

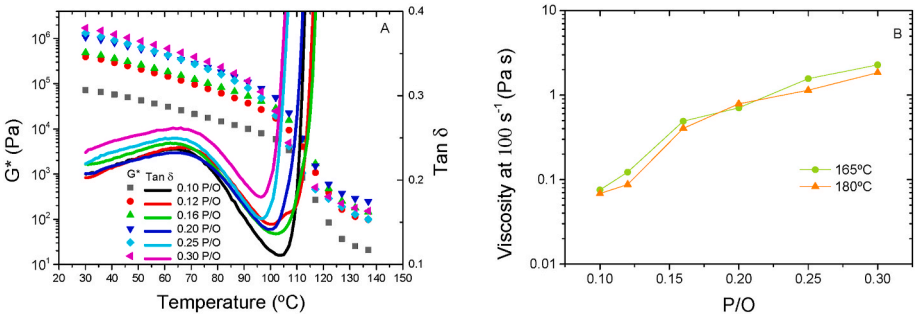

Fig. 3. A) Dependence on temperature of complex modulus (G*) and loss tangent (Tan δ = G"/G') for polymer/oil blends as a function of P/O ratio. B) Viscosity of polymer/oil blends, as a function of P/O ratio, measured at 180 °C and 100s^{-1}.

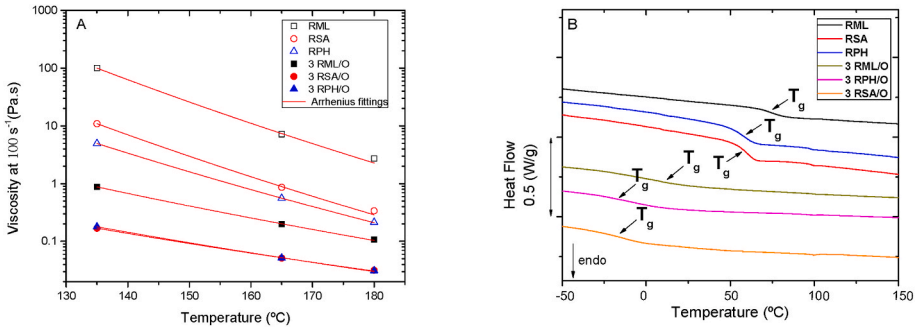

Fig. 4. Pure rosins and rosin/oil (R/O = 3) blends: A) Viscosity values at 100 $s^{-1}$and B) DSC scans.

Table 5
Activation energies (E_a) calculated from viscosity Arrhenious-like dependence on temperature and glass transition temperatures (T_g) from DSC scans for pure rosins and rosin/oil (R/O = 3) blends.

Pure rosin	E_a (kJ/mol)	T_g (°C)
RML	129.08 ± 2.13	70.2 ± 0.4
RSA	124.15 ± 2.49	60.8 ± 0.6
RPH	107.91 ± 1.15	62.6 ± 0.8
Rosin/Oil blends		
3RML/O	73.03 ± 1.56	9.9 ± 0.6
3RSA/O	58.33 ± 2.12	−15.4 ± 0.5
3RPH/O	60.94 ± 1.98	−14.8 ± 0.5

blend with P/O ratio of 0.25. As a result, R/O ratio of the resultant blends rose from 0 to 3, whereas polymer concentration decreased from 20 to 6.6% P. Table 2 gathers compositions of ternary blends formulated with RSA and RPH, rosins with similar viscosity and softening point. RML was found to be highly incompatible with the polymer fraction of the ternary blend, as will be discussed later, undergoing a fast phase separation of the polymeric fraction. As a result, this rosin was not included in this part of the study.

Fig. 5A displays oscillatory frequency sweep tests conducted on ternary blends at 60 °C. Mechanical spectra of all samples showed a predominantly elastic behavior, being values of storage modulus (G′) higher than loss modulus (G″) in the whole frequency range studied. This elastic behavior is characterized by a well-developed plateau in G′, typical of a gel-like viscoelastic behavior. Interestingly, at high polymer concentrations (i.e. low R/O ratios), in agreement with P/O binary blend (R/O = 0), G' exhibits two regions with a low frequency dependence (i.e. plateau regions) located at high and low frequencies, and a transition between them at intermediate frequencies. This viscoelastic behavior, with multiple plateaus, has been described for other binary and ternary blends, and would result from different species of entanglements. At high frequency, they would be related to the compound with the highest molecular weight (e.g. between $LDPE_r$ molecules), being effective at lower frequencies those of polymer-rosin or rosin-rosin. In all cases, oil would act as a low molecular weight solvent, not participating in the entanglements at all (Ferry, 1980).

Furthermore, G" appears to be more sensitive to this behavior, showing a plateau region at high frequencies followed by a continuous decay in its values as frequency decreases (Fig. 5A). Likewise, this viscoelastic response is also characterized by a maximum in loss tangent (result no shown), like that observed in Fig. 3A. Therefore, the observed transition seems to be mainly related to the relaxation of the polymer-rich matrix that would modify its mobility at intermediate frequencies (corresponding to the medium to high temperature region in Fig. 3A), rising its elastic characteristic and, therefore, storing more mechanical energy.

As rosin/oil ratio increases up to R/O = 2.1 (or polymer concentration is lower, around 8% P) the observed plateau in G″ becomes narrower (shifting towards higher frequencies) and, eventually, vanishes in both resins for the highest R/O ratios, being polymer concentrations in the range of 7–6% P (Fig. 5A). Therefore, viscoelastic responses are less affected by the polymer rich phase as R/O is higher. As seen in Fig. 5B, the addition of phenolic rosin (RPH) induces an initial decrease in complex modulus respect to the polymer-oil blend, but G* remains almost constant for R/O values below 1.5. Above this ratio, material exhibits lower moduli and a more viscous character, rising Tan δ = G"/G' values. In blends containing RSA, the reduction in complex shear modulus starts at lower rosin concentrations (for R/O > 1) and occurs more gradually, with higher values of G* if compared to RPH.

The microstructure observed by optical microscopy shows an extended polymer-rich phase at low rosin ratios (Fig. 6A), visible in cross-polarized pictures as light-colored polymeric regions (Fig. 6B). Conversely, disperse polymeric phases are clearly visible in Fig. 6C–F for high rosin content blends, where the rosin and oil are expected to be the continuous phase. Comparing disperse phases formed by RPH and RSA rosins, the former induces a high dispersion where crystalline polymeric fractions mostly appear as small droplets apparently not interconnected (Fig. 6D). On the contrary, polymer-rich phases formed in RSA ternary blends are of fibrillar type with interconnected regions (Fig. 6F). As a

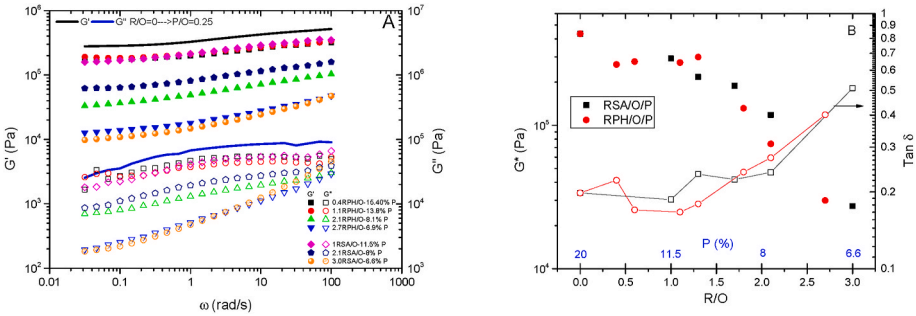

Fig. 5. RPH/O/P and RSA/O/P blends: A) Storage (G′) and loss (G″) moduli mechanical spectra, and B) Complex modulus (G*) and loss tangent (Tan δ) at 10 rad/s as a function of R/O ratio.

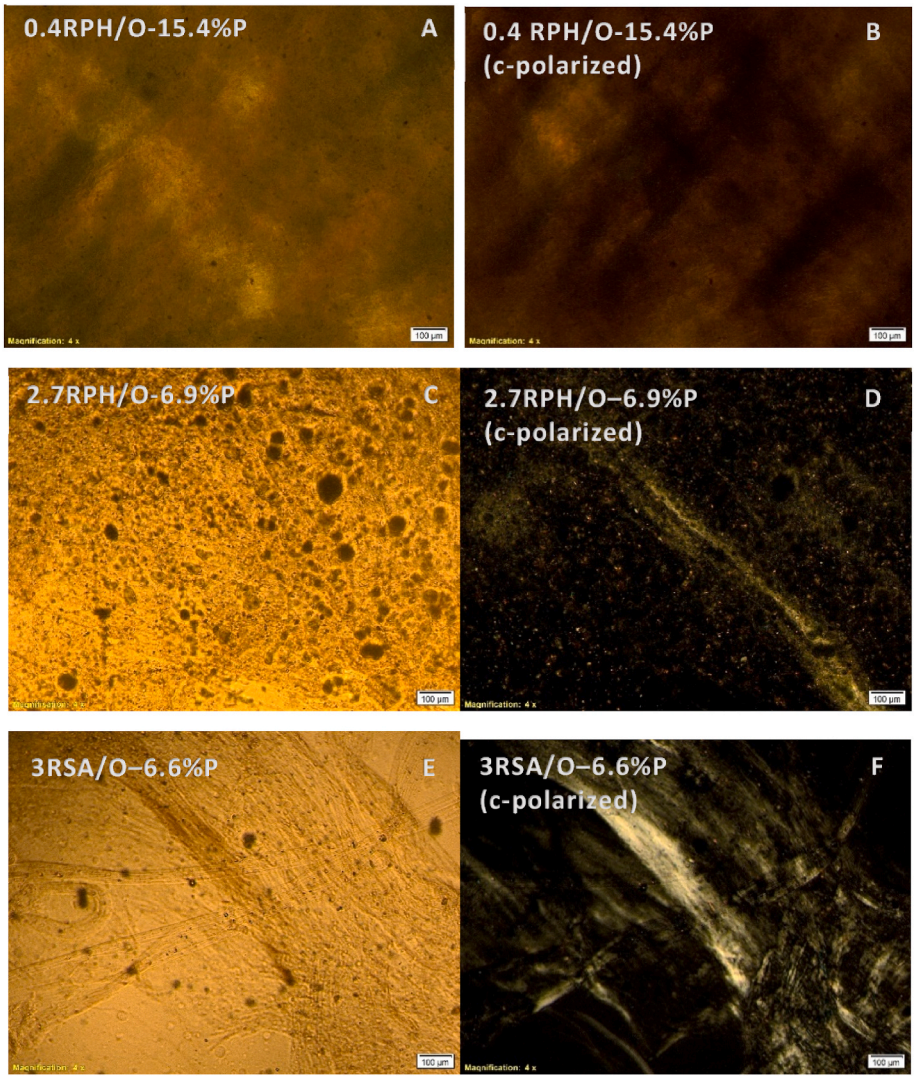

Fig. 6. Optical micrographs of selected Rosin/Oil/Polymer blends.

result, although RSA blends would evolve towards a disperse polymer-rich for R/O > 1, their shear complex modulus values reduce more gradually due to rosin-oil continuous phase plays a more predominant role in the viscoelastic behavior (Fig. 5). In this respect, the fibrillar-type microstructure observed in Fig. 6F, compared to RPH blend with similar R/O ratio, would explain the higher values of G* found for RSA/O/P ternary systems at R/O > 1 (Fig. 5B).

3.4. Non-bituminous binders

Among ternary blends previously studied, two systems (2.7RPH/O-6.9%P and 3.0RSA/O-6.6%P) exhibited enough stiffness to be considered as potential binders (referred to as B-2.7RPH/O-6.9%P and 3.0RSA/O-6.6%P in Table 3), but their softening points were too low to be applied as roofing materials. Thus, other six ternary blends were proposed as potential non-bituminous binders to study the effect of polymer concentration, rosin ratio and type. Thus, binders with a rosin/oil ratio of 2 and two polymer concentration (8.7 and 6.0% P) were formulated with the three rosins (Table 3). According to previous results, the highest polymer concentration would correspond to a range where viscoelasticity is controlled by the polymeric network, whereas rheological response for the lowest concentration was expected to be controlled by the oil/rosin fraction (Fig. 5A).

However, results have shown that this assumption also depends on the type of rosin and rosin/oil ratio used, as may be seen in Fig. 6. Thus, for blends with R/O = 2, Fig. 7B only shows the characteristic maximum in loss tangent for samples formulated with rosins RSA and RPH, which previously was related to the presence of well-developed polymer-rich phase. Conversely, binders formulated with the maleic-modified rosin ester (RML) present a continuous increase in shear complex modulus and loss tangent with frequency (Fig. 7). Furthermore, these systems are characterized by a less elastic character, compared with the other rosins (Fig. 7B), and by quick polymer phase separation during binder cooling after its high temperature processing. As a result, it is likely RML induces strong incompatibilities in the ternary blend.

Aiming to further assess the compatibility among three binder compounds, Fig. 8 displays DSC tests conducted on all materials. Scans show the endothermic event at c. a. 100 °C previously related to melting of partially crystalline swollen polymer (Fig. 2). Interestingly, the low-temperature melting process observed in polymer-oil blends, and related to the presence of free oil, has been replaced by a glass transition event, suggesting an oil/rosin compatibilization in all cases.

Likewise, rosins RPH and RSA seem to improve compatibility with polymer when mixed at R/O = 2. As may be seen in Table 4, crystallization degrees (X_c) measured in binders formulated with both rosins are lower than those corresponding to polymer-oil blends with similar $LDPE_r$ concentration. Nevertheless, the opposite effect is observed for RML with a crystallization degree rising up to $X_c \approx 32\%$, close to that

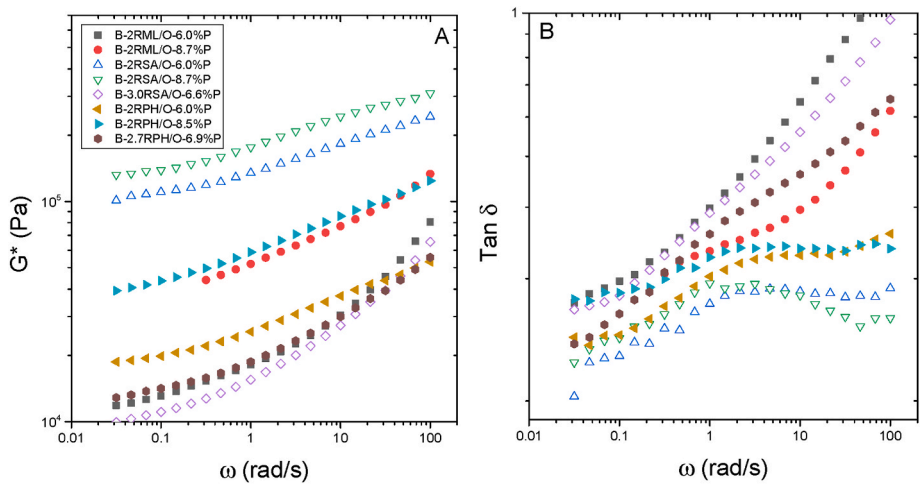

Fig. 7. A) Complex modulus (G*) and B) loss tangent (Tan δ) curves for selected binders.

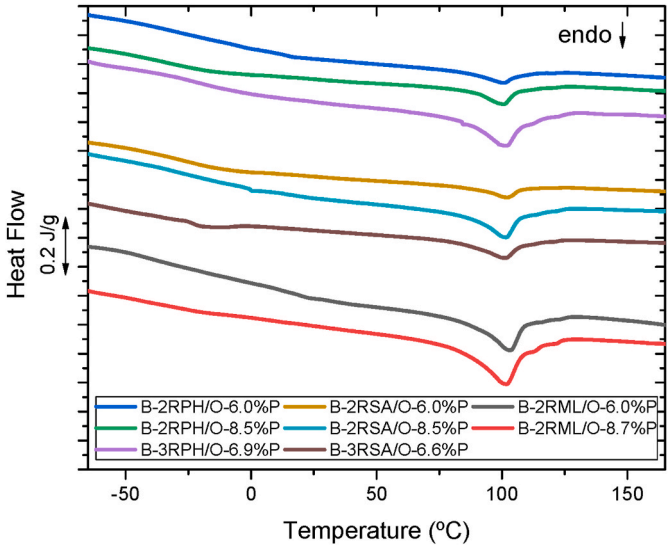

Fig. 8. DSC scans obtained for selected Rosin/Oil– Polymer Binders.

measured for the recycled $LDPE_r$ (X_c = 34%). This fact would confirm the above-commented incompatibility induced by this rosin. Furthermore, comparing RSA and RPH-formulated systems with a R/O fixed at 2, the RPH/O phase seems to be slightly more compatible with $LDPE_r$, with melting temperatures, T_m, closer to those found for P/O systems (Table 4).

If only those more compatible rosins are considered, RSA-formulated binders showed the highest moduli and the lowest loss tangent values, being this rosin less affected by the polymer concentration, i.e. RSA induces smaller changes in G* and Tanδ than RPH (Fig. 7). Interestingly, softening points measured in binders (Table 3) do not agree with their viscoelastic moduli that depend on polymer concentration and rosin type. For a ratio R/O = 2, binders formulated with RPH show higher softening points than RSA derived systems, which seems to be related to compatibility among $LDPE_r$ and the other two compounds, and differences in microstructure previously observed (Fig. 6). Thus, it was visually observed that RPH-formulated samples presented more elongation during ring & ball softening point tests, delaying ball drop and, therefore, increasing softening temperature. Conversely, the fibrillar-type microstructure expected in RSA-formulated binders hardly exhibited elongation capability during the softening point test, giving rise to an early binder breaking and ball drop. Finally, compatibility is also dependent on R/O ratio, decreasing as rosin concentration is higher (i.e. crystallinity degree and melting temperature rise for R/O = 3, as seen in Table 4). Furthermore, binders softening points are lower in both cases (Table 3), compared with systems containing less polymer concentration (e.g. binders B-2RPH/O-6.0%P and B-2RSA/O-6.0%P). These results would agree with a disperse polymer-rich phase organized as small droplets apparently not interconnected, as seen in Fig. 6D for RPH formulated systems, where rheological behavior is controlled by the oil-rosin phase (Fig. 7).

In addition to the above characterization, performed to stablish in-service material performance, Fig. 9A displays the flow behavior of selected binders at 180 °C. This is the processing temperature and, likely, will be used during manufacture of roofing membranes. Despite the high testing temperature, all binders behave as non-Newtonian fluids, exhibiting a shear-thinning behavior, but with relatively low viscosities in the range of shear rates studied (between 0.2 and 0.03 Pa s). As the above observed viscous behavior of R/O blends, binder viscosities present an Arrhenius-like temperature dependence from 135 to 180 °C, showing higher viscosity those binders formulated with RPH (Fig. 9B). However, activation energies calculated for binders were slightly lower than those measured for the R/O blends (Fig. 9B and Table 5), likely due to polymer addition that was previously seen to reduce viscosity dependence on temperature (Fig. 3B).

On these grounds, attending to compatibility of RPH with oil and polymer, and softening points measured (Table 3), B-2RPH/O-6.0%P and B-2RPH/O-8.5%P were proposed as potential non-bituminous binders for roofing, according to the ASTM standard D312. This specification is used to classify four types of bitumens for use in built-up roof construction, construction of some modified bitumen systems, construction of bituminous vapor retarder systems, and for adhering insulation boards used in various types of roof systems. In this regard, both RPH-based binders showed softening points around 108 °C, and penetrations of 54 and 28 dmm, respectively for B-2RPH/O-6.0%P and B-2RPH/O-8.5%P. Considering these characteristics, binder B-2RPH/O-6.0%P would be approximately classified as Type IV that requires a softening point values between 99 and 107 °C, penetrations from 12 to 25 dmm and a minimum ductility at 25 °C of 1.5 cm.

3.5. Heat radiation absorption

Sun radiation is absorbed by roofing materials, but the amount of heat transfer depends on the surface material and color, as well as the wavelength of the incoming radiation (Aletba et al., 2021). Unlike black color bituminous binders, these materials have light yellowish to brownish color (Fig. 10), with promising characteristics to be used in

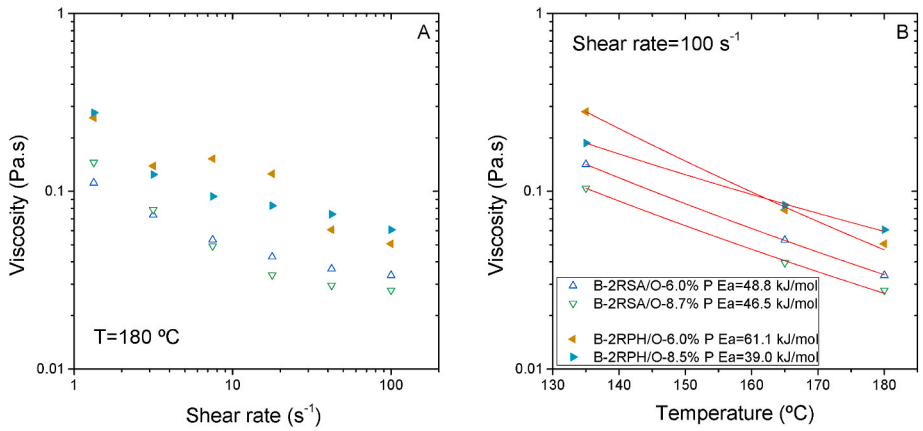

Fig. 9. Viscous flow behavior (A) and viscosity values at 100 s^{-1} as function of temperature (B) for selected Rosin/Oil– Polymer binders.

reflective roof surfaces that will comply with industry reflectivity requirements, reduce the heat island effect, and save energy. According to previous results, B-2RPH/O-8.5%P was selected to assess its ability to absorb solar radiation, in comparison with a black bituminous binder, a polymer modified bitumen with 75 °C softening point and 43 dmm penetration.

To that end, the experimental setup previously described, and sketched in Fig. 10A, was used to apply two mean radiant flux densities, q*, of 924 and 1266 W/m^2. The latter close to the maximum solar radiation expected in warm climates (Pisello et al., 2017). During the experiment, the radiation reaching the top surface of the sample is partially absorbed (and heat is conducted through the material), and the rest is reflected, emitted as heat radiation and lost by free convection. As a result, top surface of the material increases its temperature (T_{top}) and a temperature gradient between the top and bottom of the sample is recorded along testing time, referred to as (T_{top}-T_{bottom}) in Fig. 10A. As may be seen for the modified bitumen submitted to q*≈924 W/m^2, top temperature of the sample undergoes an initial increase followed to a trend to reach a constant value around 59 °C. This value is about 35 °C higher than the selected temperature of the surroundings that was set at 25 °C, and agrees with results reported by other authors in bituminous materials (Aletba et al., 2021). Similarly, bitumen top temperature significantly rises to 74 °C when q*≈1266 W/m^2, which was 8 °C higher than the temperature recorded for the non-bituminous binder that reached a value for T_{top} of 66 °C.

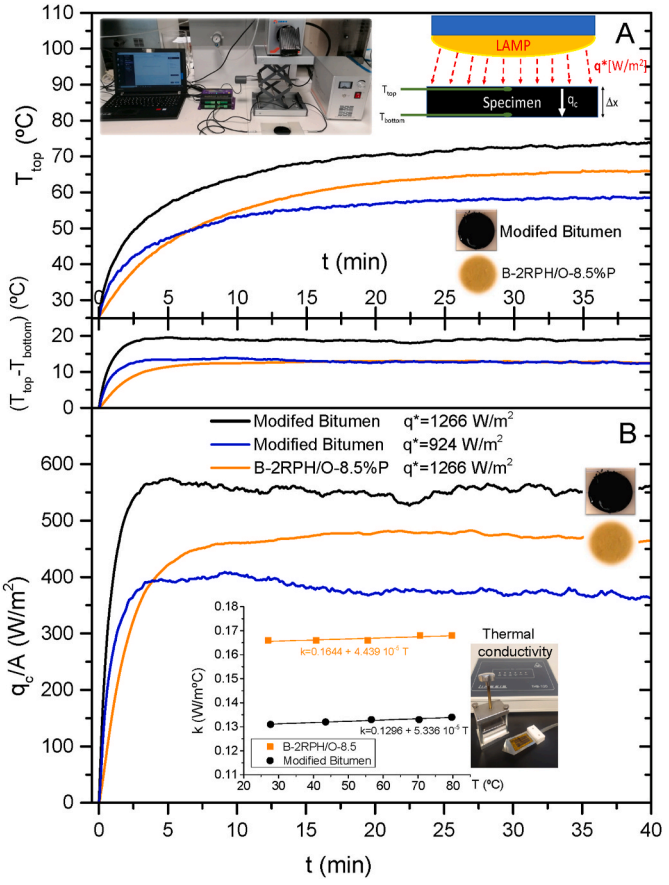

Fig. 10. A) Thermal radiation setup (inset) and material temperatures recorded with time as a function of irradiance flux density (q*); and B) Heat flux (q_c/A) conducted through the sample and thermal conductivity tests and device (inset).

At the same time, after an initial increase, temperature gradient (T_{top}-T_{bottom}) also reaches constant values that depend on radiation intensity and material (Fig. 10A). Thus, at 1266 W/m^2, temperature gradients are about 20 °C and 12 °C, respectively, for the polymer-modified bitumen and the non-bituminous binder. The latter is the same temperature gradient observed for bitumen subjected to q*≈924 W/m^2. Moreover, the constant gradients recorded with time mean that a steady heat flux (q_c/A) is conducted through the sample, which can be calculated by the Fourier law, as follows:

$$\frac{q_c}{A} = k\frac{(T_{top} - T_{bottom})}{\Delta x} \quad (2)$$

where k is material thermal conductivity (W/m°C) and Δx (m) is specimen thickness (or distance between temperature sensors) that was 4.54 mm. To obtain k, thermal conductivity tests were performed on reference bitumen and on the selected non-bituminous binder within the tested experimental range, 30–80 °C (inset in Fig. 10B). As may be seen, thermal conductivities of modified bitumen ranged between 0.131 ± 0.001 and 0.134 ± 0.001 W/m °C. On the other hand, system B-2RPH/O-8.5%P presented about 25% higher thermal conductivity than bitumen, changing from 0.166 ± 0.001 to 0.168 ± 0.001 W/m °C within the same range of testing temperatures.

Using above thermal conductivities and temperature gradients recorded for every material and radiation intensity applied, heat fluxes (q_c/A) conducted through the sample were calculated using Equation (2), and are displayed in Fig. 10B. Under a theoretical maximum solar radiation, q*≈924 W/m^2, bitumen absorbs an average heat flux of 376.7 ± 9.3 W/m^2, whereas this value increases up to 552.3 ± 7.9 W/m^2 for q*≈1266 W/m^2. This means that selected bitumen is able to absorb around 30% of peak incident radiation, 1282 and 1752 W/m^2 respectively, measured at sample center. Interestingly, average heat flux conducted through the non-bituminous binder was lower, 473.2 ± 5.7

W/m^2 for $q^* \approx 1266$ W/m^2. In this case, non-bituminous binder is able to absorb around 27% of peak incident thermal radiation, i.e. heat conducted through the roofing material into the building could be reduced by up to 14%, compared with a black bituminous material.

4. Conclusions

Three bio-based rosin esters (R), a waste cooking oil (O) and a polyethylene recycled ($LDPE_r$) have been used in binder formulations. Results have shown a partial compatibility between the $LDPE_r$ and oil that gives rise to a polymer-rich phase, involving a swelling process that modifies polymer crystallinity (i.e. decreasing melting temperature and crystallization degree), and a physical retention of free oil that appears as a low-temperature melting event in DSC scans. Conversely, all rosins and oil forms compatible blends where rosin glass transition temperature is shifted to lower values (between 10 and -15 °C) and the low-temperature melting event related to free oil vanishes. Finally, ternary blends formulated with rosins RPH and RSA seem to improve compatibility with polymer when mixed at R/O = 2. Crystallization degrees measured in binders formulated with both rosins are lower than those corresponding to polymer-oil blends containing similar $LDPE_r$ concentration.

Material stiffness (viscoelasticity and penetration test) and softening point will result from the final compatibility reached among three compounds, and microstructure developed. For a ratio R/O = 2, binders formulated with RPH show higher softening points than RSA derived systems. RPH-formulated samples presented more elongation during ring & ball softening point tests, delaying ball drop and, therefore, increasing softening temperature. Conversely, the fibrillar-type microstructure expected in RSA-formulated binders hardly exhibited elongation.

As a result, a binder formulated with 61.0% phenolic-modified rosin, 30.5% oil and 8.5% $LDPE_r$ has shown suitable mechanical properties for roofing materials, classified as Type IV according to ASTM D312 standard, and has exhibited enhanced energy efficiency derived from its light yellowish to brownish color. Under the experimental radiant flux conditions, surface temperature of the non-bituminous binder was 8 °C lower than that of the black bitumen. Moreover, conduction heat transfer through this roofing material was about 14% lower than that conducted through a bitumen-based membrane with the same thickness. Developed binders are expected to behave as reflective building materials aiming to reduce the heat island effects and save energy. In any case, further work is still necessary to stablish the final use of these materials that, among others, will depend on their response against long-term aging, processability and applicability on binders-fillers mixes, etc. Additionally, a comprehensive life cycle assessment should be carried out to establish the actual reduction in carbon emissions resulting from the production and use of these materials.

CRediT authorship contribution statement

R. Álvarez-Barajas: Investigation, Formal analysis, Data curation, Writing – original draft. **A.A. Cuadri:** Investigation, Data curation, Methodology, Writing – review & editing. **C. Delgado-Sánchez:** Investigation, Data curation. **F.J. Navarro:** Investigation, Data curation. **P. Partal:** Conceptualization, Methodology, Writing – review & editing, Supervision, project acquisition, Funding acquisition.

Declaration of competing interest

The authors declare that they have no known competing financial interests or personal relationships that could have appeared to influence the work reported in this paper.

Data availability

The data that has been used is confidential.

Acknowledgements

This work is part of GreenAsphalt project (ref. 802C1800001), co-funded by FEDER European Programme (80%) and Junta de Andalucía (Consejería de Economía, Conocimiento, Empresas y Unversidades/ Agencia-IDEA), and has been also co-funded by FEDER/Junta de Andalucía-Consejería de Economía y Conocimiento/Project UHU-1256916. Clara Delgado-Sánchez also acknowledges financial support from Junta de Andalucía through post-doctoral Grant No. DC 01228 (PAIDI 2020), co-funded by the EU Fondo Social Europeo (FSE). Funding for open access charge: Universidad de Huelva / CBUA.

References

Aldas, M., Pavon, C., López-Martínez, J., Arrieta, M.P., 2020. Pine resin derivatives as sustainable additives to improve the mechanical and thermal properties of injected moulded thermoplastic starch. Appl. Sci. 10, 2561. https://doi.org/10.3390/app10072561.

Aletba, S.R.O., Hassan, N.A., Jaya, R.P., Aminudin, E., Mahmud, M.Z.H., Mohamed, A., Hussein, A.A., 2021. Thermal performance of cooling strategies for asphalt pavement: a state-of-the-art review. J. Traffic Transport. Eng. 8, 356–373. https://doi.org/10.1016/j.jtte.2021.02.001.

Badin, G., Ahmad, N., Muhammad, H., Ahmad, T., Sohail, M., 2021. Effect of addition of pigments on thermal characteristics and the resulting performance enhancement of asphalt. Construct. Build. Mater. 302, 124212 https://doi.org/10.1016/j.conbuildmat.2021.124212.

Bianchini, F., Hewage, K., 2012. How " green " are the green roofs? Lifecycle analysis of green roof materials. Build. Environ. 48, 57–65. https://doi.org/10.1016/j.buildenv.2011.08.019.

Boixo, S., Diaz-vicente, M., Colmenar, A., Alonso, M., 2012. Potential energy savings from cool roofs in Spain and Andalusia. Energy 38, 425–438. https://doi.org/10.1016/j.energy.2011.11.009.

Brännström, H., Kumar, H., Álen, R., 2018. Current and potential biofuel production from plant oils. BioEnergy Res 11, 592–613. https://doi.org/10.1007/s12155-018-9923-2.

Burkhanovich, S.S., 2022. Creation of polymer bitumen compositions for roofing based on local raw materials. Oriens 2, 60–66. https://doi.org/10.5281/zenodo.6993973.

Cascone, S., Ingrao, C., Valenti, F., Porto, S.M.C., 2020. Energy and environmental assessment of plastic granule production from recycled greenhouse covering films in a circular economy perspective. J. Environ. Manag. 254, 109796 https://doi.org/10.1016/j.jenvman.2019.109796.

Cuadri, A.A., Roman, C., García-Morales, M., Guisado, F., Moreno, E., Partal, P., 2016. Formulation and processing of recycled-low-density-polyethylene-modified bitumen emulsions for reduced-temperature asphalt technologies. Chem. Eng. Sci. 156, 197–205. https://doi.org/10.1016/j.ces.2016.09.018.

Ebnesajjad, S., Morgan, R., 2012. Applications of processing aid additives. In: Fluoropolymer Additives, pp. 193–209. https://doi.org/10.1016/B978-1-4377-3461-4.00011-8.

Ferdous, W., Manalo, A., Aravinthan, T., Van Erp, G., 2016. Properties of epoxy polymer concrete matrix: effect of resin-to-filler ratio and determination of optimal mix for composite railway sleepers. Construct. Build. Mater. 124, 287–300. https://doi.org/10.1016/j.conbuildmat.2016.07.111.

Ferry, J.D., 1980. Viscoelastic Properties of Polymers, third ed. Jonh Wiley & Sons, New York.

Fuentes-Audén, C., Martínez-Boza, F.J., Navarro, F.J., Partal, P., Gallegos, C., 2005. Viscous flow properties and phase behaviour of oil–resin blends. Fluid Phase Equil. 237, 117–122. https://doi.org/10.1016/j.fluid.2005.08.017.

Fuentes-Audén, C., Martínez-Boza, F.J., Navarro, F.J., Partal, P., Gallegos, C., 2007. Formulation of new synthetic binders: thermo-mechanical properties of recycled polymer/oil blends. Polym. Test. 26, 323–332. https://doi.org/10.1016/j.polymertesting.2006.11.002.

Fuentes-Audén, C., Sandoval, J.A., Jerez, A., Navarro, F.J., Martínez-Boza, F.J., Partal, P., Gallegos, C., 2008. Evaluation of thermal and mechanical properties of recycled polyethylene modified bitumen. Polym. Test. 27, 1005–1012. https://doi.org/10.1016/j.polymertesting.2008.09.006.

Garrido, M., António, D., Lopes, J.G., Correia, J.R., 2018. Performance of different joining techniques used in the repair of bituminous waterproofing membranes. Construct. Build. Mater. 158, 346–358. https://doi.org/10.1016/j.conbuildmat.2017.09.180.

Gordon, M., Taylor, J.S., 1952. Ideal copolymers and the second-order transitions of synthetic rubbers. i. non-crystalline copolymers. J. Appl. Chem. 2, 493–500. https://doi.org/10.1002/jctb.5010020901.

Iqbal, S., Jehan, B., Khan, F.A., Nasir, H., Khan, S.A., Khan, S.A., 2019. Assessment of roof waterproofing by pre-packaged polymer modified slurry (PPPMS) and bitumen. Adv. Environ. Res. 8, 71–84. https://doi.org/10.12989/aer.2019.8.1.071.

Joni, H.H., Al-Rubaee, R.H.A., Al-Zerkani, M.A., 2020. Characteristics of asphalt binder modified with waste vegetable oil and waste plastics. IOP Conf. Ser. Mater. Sci. Eng. 737, 012126 https://doi.org/10.1088/1757-899X/737/1/012126.

Kazemi, M., Fini, E.H., 2022. State of the art in the application of functionalized waste polymers in the built environment. Resour. Conserv. Recycl. 177, 105967 https://doi.org/10.1016/j.resconrec.2021.105967.

Kugler, S., Ossowicz, P., Malarcyzyk-Matusiak, K., Wierzbicka, E., 2019. Advances in rosin-based chemicals: the latest recipes, applications and future trends. Molecules 24, 1651. https://doi.org/10.3390/molecules24091651.

Li, D., Zhou, L., Wang, X., He, L., Yang, X., 2019. Effect of crystallinity of polyethylene with different densities on breakdown strength and conductance property. Materials 12, 1746. https://doi.org/10.3390/ma12111746.

Meisenheimer, H., Zens, A., 2008. Ethylene vinyl acetate elastomer (EVM) (ASTM designation AEM). In: Robert C. Klingender, Handbook of Specialty Elastomer. CRC Press/Taylor & Francis, Boca Raton.

Munera, J.C., Ossa, E.A., 2014. Polymer modified bitumen: optimization and selection. Mater. Des. 62, 91–97. https://doi.org/10.1016/j.matdes.2014.05.009.

Muruzina, E.V., Murzagalina, E.I., 2020. Study of the eco-friendly roofing materials based on elastomers in accelerated modes. Procedia Environ. Sci. 7, 571–579.

Navarro, F.J., Partal, P., Martínez-Boza, F.J., Gallegos, C., 2005. Effect of composition and processing on the linear viscoelasticity of synthetic binders. Eur. Polym. J. 41, 1429–1438. https://doi.org/10.1016/j.eurpolymj.2004.12.006.

Navarro, F.J., Partal, P., Martínez-Boza, F.J., Gallegos, C., 2010. Novel recycled polyethylene/ground tire rubber/bitumen blends for use in roofing applications: thermo-mechanical properties. Polym. Test. 29, 588–595. https://doi.org/10.1016/j.polymertesting.2010.03.010.

Okhotnikova, E.S., Ganeeva, Y.M., Frolov, I.N., Yusupova, T.N., Fazylzyanova, G.R., 2022. Structural characterization and application of bitumen modified by recycled polyethylenes. Construct. Build. Mater. 316, 126118 https://doi.org/10.1016/j.conbuildmat.2021.126118.

Pan, F., Pei, J., Zhang, G., Wen, Y., Zhang, J., Li, R., 2022. Building the cooling roads with high thermal conductivity pavements to relieve urban heat island effect. Construct. Build. Mater. 346, 128276 https://doi.org/10.1016/j.conbuildmat.2022.128276.

Partal, P., Martìnez-Boza, F.J., Conde, B., Gallegos, C., 1999. Rheological characterisation of synthetic binders and unmodified bitumens. Fuel 78, 1–10. https://doi.org/10.1016/S0016-2361(98)00121-5.

Pisello, A.L., Castaldo, V.L., Piselli, C., Fabiani, C., Cotana, F., 2017. Thermal performance of coupled cool roof and cool façade: experimental monitoring and analytical optimization procedure. Energy Build. 157, 35–52. https://doi.org/10.1016/j.enbuild.2017.04.054.

Ribeiro, A.P., Masuchi, M.H., Miyasaki, E.K., Domingues, M.A., Stroppa, V.L., de Oliveira, G.M., Kieckbusch, T.G., 2015. Crystallization modifiers in lipid systems. J. Food Sci. Technol. 52, 3925–3946. https://doi.org/10.1007/s13197-014-1587-0.

Rodríguez-Gómez, J.E., Silva-Reynoso, Y.Q., Varela-Guerrero, V., Núñez-Pineda, A., Barrera-Díaz, C.E., 2015. Development of a process using waste vegetable oil for separation of aluminum and polyethylene from Tetra Pak. Fuel 149, 90–94. https://doi.org/10.1016/j.fuel.2014.09.032.

Rupal, A., Sharma, S.K., Tyagi, G.D., 2020. Experimental investigation on mechanical properties of polyurethane modified bituminous waterproofing membrane. Mater. Today Proc. 27, 467–474. https://doi.org/10.1016/j.matpr.2019.11.278.

Senise, S., Carrera, V., Navarro, F.J., Partal, P., 2017. Thermomechanical and microstructural evaluation of hybrid rubberised bitumen containing a thermoplastic polymer. Construct. Build. Mater. 157, 873–884. https://doi.org/10.1016/j.conbuildmat.2017.09.126.

Shen, J., Liang, J., Lin, X., Lin, H., Yu, J., Yang, Z., 2020. Recent progress in polymer-based building materials. Int. J. Polym. Sci. https://doi.org/10.1155/2020/8838160, 8838160.

Shittu, E., Stojceska, V., Gratton, P., Kolokotroni, M., 2020. Environmental impact of cool roof paint : case-study of house retrofit in two hot islands. Energy Build. 217, 110007 https://doi.org/10.1016/j.enbuild.2020.110007.

Silvestre, A.J.D., Gandini, A., 2008. Rosin: major sources, properties and applications. In: Monomers, Polymers and Composites from Renewable Resources, pp. 67–88. https://doi.org/10.1016/B978-0-08-045316-3.00004-1.

Tolinski, M., 2009. Trends in polyolefin and additive use. In: Additives for Polyolefins. Elsevier Inc., pp. 9–21. https://doi.org/10.1016/B978-0-8155-2051-1.00002-9

Wypych, G., 2020. Handbook of UV Degradation and Stabilization, third ed. ChemTec Publishing. https://doi.org/10.1016/B978-1-927885-57-4.50013-9.

Xu, Z., Lou, W., Zhao, G., Zhang, M., Hao, J., Wang, X., 2019. Pentaerythritol rosin ester as an environmentally friendly multifunctional additive in vegetable oil-based lubricant. Tribol. Int. 135, 213–218. https://doi.org/10.1016/j.triboint.2019.02.038.

Yuliestyan, A., Cuadri, A.A., García-Morales, M., Partal, P., 2016. Influence of polymer melting point and Melt Flow Index on the performance of ethylene-vinyl-acetate modified bitumen for reduced-temperature application. Mater. Des. 96, 180–188. https://doi.org/10.1016/j.matdes.2016.02.003.

Yuliestyan, A., Gabet, T., Marsac, P., García-Morales, M., Partal, P., 2018. Sustainable asphalt mixes manufactured with reclaimed asphalt and modified-lignin-stabilized bitumen emulsions. Construct. Build. Mater. 173, 662–671. https://doi.org/10.1016/j.conbuildmat.2018.04.044.

Zakaria, F., Radwan, M.A., Sadek, M.A., Elazab, H.A., 2018. Insulating material based on shredded used tires and inexpensive polymers for different roofs. Int. J. Eng. Tecnol. 7, 1983–1988. https://doi.org/10.14419/ijet.v7i4.14081.